Comparison of Volcanic Explosions in Japan Using Impulsive Ionospheric Disturbances

Mokhamad Nur Cahyadi (cahyadi@geodesy.its.ac.id)
Institut Teknologi Sepuluh Nopember Fakultas Teknik Sipil dan Perencanaan https://orcid.org/0000-0002-0549-0606

Eko Yuli Handoko
Institut Teknologi Sepuluh Nopember

Ririn Wuri Rahayu
Institut Teknologi Sepuluh Nopember

Kosuke Heki
Hokkaido University

Research Article

Keywords: Ionospheric disturbance, Asama, Shin-Moe Sakurajima, Kuchinoerabu-jima, volcanic explosion, GNSS-TEC.

Posted Date: July 16th, 2021

DOI: https://doi.org/10.21203/rs.3.rs-707713/v1

Version of Record: A version of this preprint was published at Earth, Planets and Space on December 1st, 2021. See the published version at https://doi.org/10.1186/s40623-021-01539-5.

Abstract

Using the total ionospheric electron content (TEC) data from ground-based global satellite navigation system (GNSS) receivers in Japan, we compared ionospheric responses to five explosive volcanic eruptions 2004-2015 of the Asama, Shin-Moe, Sakurajima, and Kuchinoerabu-jima volcanoes. The TEC records show N-shaped disturbances with a period ~80 seconds propagating outward with the acoustic wave speed in the F region of the ionosphere. The amplitudes of these TEC disturbances are a few percent of the background absolute vertical TEC. We propose to use such relative amplitudes as a new index for the intensity of volcanic explosions.

1. Introduction

The Earth's ionosphere ranges from ~ 60 to > 800 km in altitude and is characterized by large number of free electrons. Ionospheric conditions are controlled by solar radiation and often disturbed by geomagnetic activities. In addition to such disturbances caused by space weather, the ionosphere is disturbed by events below (Blanc, 1985), such as earthquakes (Astafyeva and Heki, 2009; Komjathy et al, 2013; Heki, 2021), tsunami (Occhipinti et al., 2013), human-induced explosions (Kundu et al., 2020), and volcanic eruptions.

Ionospheric total electron content (TEC) can be easily measured by comparing the phases of two microwave carriers from global navigation satellite system (GNSS) satellites, such as Global Positioning System (GPS) (e.g. Hofmann-Wellenhof et al., 2008). Ground GNSS networks have been deployed to monitor crustal movements, and these networks were found useful to study ionospheric disturbances by volcanic eruptions. There are two types of ionospheric TEC responses to various types of volcanic eruptions.

The first type is the long-lasting harmonic TEC oscillations (Fig. 1). They are atmospheric modes excited by continuous acoustic waves generated typically by Plinian eruptions. They have prescribed frequencies reflecting the vertical atmospheric structure. It was found after the 13 July 2003 eruption of the Soufrière Hills volcano, Montserrat, in the Lesser Antilles (Dautermann et al., 2003a, b), and after the February 2014 eruption of the Kelud volcano, eastern Java Island, Indonesia (Nakashima et al., 2016). They reported that harmonic oscillations caused by atmospheric resonance excited by the Plinian eruption of the Kelud volcano lasted for ~ 2.5 hours after the eruption started. Shults et al. (2016) found similar TEC oscillations after the 2015 April Plinian eruption of the Calbuco volcano, Chile. Cahyadi et al. (2020) also found such harmonic TEC oscillations lasting ~ 20 minutes following the 2010 November 5 eruption of the Merapi volcano, central Java Island. Although the onsets of these continuous eruptions are not always clear, the TEC oscillations emerge 20–30 minutes after the eruptions started. Cahyadi et al. (2020) also suggested that the TEC oscillation amplitudes relative to background TEC represent the mass eruption rate, and the products of such amplitudes and the duration provides a new index for the total amount of the ejecta.

The second type of disturbances occur 8–10 minutes after volcanic explosions by short pulses of acoustic waves propagating upward from the surface to the ionospheric F region (Fig. 1). They make short-term N-shaped impulsive TEC responses as Heki (2006) observed with the GPS-TEC method after the Vulcanian explosive eruption of the Asama volcano, Central Japan, on September 1, 2004. Here we focus on the impulsive ionospheric responses to this type of volcanic explosions.

Intensity of a volcanic explosion has been studied by atmospheric pressure changes associated with the airwave (infrasound) generated by the eruption (e.g. Matoza et al., 2019). However, geometric settings of such sensors relative to volcanoes are diverse, and amplitudes of such airwaves are difficult to serve as a universal index to describe the explosion intensity. Volcanic explosivity index (VEI) is used to describe the intensity of the eruptions (Newhall and Self, 1982). However, this index is determined by the amount of ejecta and does not directly indicate the explosions intensities. In this study, we explore the possibility to use the amplitude of ionospheric disturbance that occur ~ 10 minutes after a large explosion as the new index. For this purpose, we compare ionospheric TEC responses to five recent explosive volcanic eruptions of four volcanoes in Japan 2004–2015 comparing the GNSS-TEC data from GEONET (GNSS Earth Observation Network), a continuous GNSS network in Japan.

2. Gnss Data

We calculated TEC by multiplying a certain factor to the phase difference of the microwave signals in two frequencies, L1 (~ 1.5 GHz) and L2 (~ 1.2 GHz), from GNSS receivers in the Japanese GEONET (here we use only GPS satellites). TEC indicates number of electrons integrated along the line-of-sight (LoS) connecting the ground stations and GNSS satellites. We often represent the point of observation using the latitude and longitude of ionospheric piercing point (IPP), the point of intersection of LoS with the hypothetical thin layer assumed at the altitude of the highest electron density (~ 300 km). This is because TEC is most sensitive to changes in the F region. We plot their surface projections, often called sub-ionospheric points (SIP), on the map.

We downloaded the raw GEONET GNSS data on the days of the eruptions from Geospatial Information Authority of Japan (https://terras.gsi.go.jp). We use the phase differences between L1 and L2 microwave carrier phases and converted them to TEC. Such slant TEC (STEC) values are often converted to vertical TEC (VTEC) after removing inter-frequency biases in GNSS receivers and satellites. Here, however, we use STEC throughout the study in order to capture TEC signatures from LoS penetrating the wavefront with shallow angles (Fig. 1). We use VTEC calculated from Global Ionospheric Map (GIM; Mannucci et al. 1998) only to normalize the amplitudes of the STEC changes with the background VTEC. The details of the GNSS-TEC technique to study lithospheric phenomena are available in the book chapter by Heki (2021).

Interaction of the electron movement with geomagnetic fields allows us to observe such TEC disturbances from stations located to the south/north of volcanoes in northern/southern hemispheres (Heki and Ping, 2005; Heki, 2006; Rolland et al., 2013; Kundu et al., 2021). Figure 2 shows an example of

the STEC change time series before and after the 2011 February 11 eruption of the Shin-Moe volcano in Kyushu, SW Japan, observed at the station 0729 located in a small island to the south of Kyushu. We cannot take advantage of the dense network because the volcano is located near the southern edge of SW Japan, and the TEC signatures are visible only at the southern side. We isolated the short-term signals by fitting the polynomials (with degree 7) to STEC time series and showing residuals from such reference curves. The degree of the polynomials is tuned so that the long-period fluctuations are effectively removed. The short-period TEC signatures made by volcanic eruptions are insensitive to the selection of the polynomial degree as demonstrated in Figure S1.

Small pulses occurring ~ 10 minutes after the eruption (Satellites 4, 10, 13) are caused by acoustic waves propagating from the volcano to the ionosphere. Incessant small fluctuations of TEC observed by Satellites 7, 8, 12, 17, and 26 are natural variabilities of TEC intrinsic for low elevation satellites. The Dst index time series shows that geomagnetic activity is low on 2011 Feb. 11 and on the other eruption days (Figure S2). Figure S3 compares the TEC data in Fig. 2 with those on the previous (2011 Feb.10) and the next (2011 Feb. 12) days of the eruption.

3. Five Volcanic Explosions Of Four Volcanoes In Japan

We selected five recent explosive volcanic eruptions in Japan with clear TEC disturbance signals. The Asama volcano, central Japan, started eruptive activity at 11:02 UT on September 1, 2004, with a Vulcanian explosion associated with strong airwaves (Nakada et al., 2005). For this eruption, there have been reports of ionospheric disturbance using GNSS-TEC by Heki (2006) and by HF-Doppler measurements by Chonan et al. (2018). Plume height was unknown due to cloudy weather, and they detected the atmospheric pressure change exceeding 205 Pa at a sensor located ~ 8 km to the south (Yokoo et al., 2005). VEI of this eruption is reported as 2 according to Global Volcanism Program (2013) (same source for VEIs of the other eruptions).

Sakurajima is an active stratovolcano in the Kagoshima Prefecture, Kyushu, and is one of the most active volcanoes in SW Japan. Since 2009, several hundreds of explosions occur every year in the volcano. There were 125 eruptions in 2009 October, in which 101 were explosive. The explosion of Minamidake, Sakurajima, at 07:45 UT on October 3, 2009, was one of the strongest eruptions in its activity since 2009. Plume reached the height ~ 3,000 m above the caldera rim, and the atmospheric pressure change exceeding 294.5 Pa was detected at a sensor ~ 5 km southeastward. At another observatory, ~ 11 km to the west of the vent, pressure change of 74 Pa was observed (JMA, 2010).

Shin-Moe Volcano is also located in the Kagoshima Prefecture, Kyushu. We studied two VEI 2 explosive eruptions in 2011. In the first eruption (Jan. 31 22:54 UT), the plume reached the height of ~ 2,000 m above the caldera rim, and the atmospheric pressure change exceeding 458.5 Pa was observed at a sensor ~ 2.6 km southwestward. In the second eruption (Feb. 11, 02:36 UT), the plume reached the height of ~ 2,500 m above the caldera rim, and the atmospheric pressure change exceeding 244.3 Pa was observed at the same sensor (JMA, 2013).

The last volcanic eruption was Kuchinoerabu-jima volcano, located at a tiny island Kuchinoerabu-jima ~ 100 km to the south of Kyushu. A VEI 3 eruption occurred on 29 May 2015 (00:59 UT). The plume height was ~ 9,000 m, and pyroclastic flow reached the ocean. An atmospheric pressure of 62.2 Pa was observed at a sensor located ~ 2.3 km northeastward (JMA, 2015). Nakashima (2018) studied ionospheric disturbances caused by this eruption by using 1 Hz high-rate GNSS data.

4. Comparison Of Ionospheric Disturbances By The Five Volcanic Explosions

Figure 3 compares the impulsive TEC changes with periods of 1-2 minutes, ~10 minutes after the explosion. They are all STEC and the time series show the residual from the best-fit polynomials with degrees 7-9. We also see faint harmonic oscillations (similar to Type 1 disturbance in Figure 1) sometimes follow the eruptions, e.g., the 2015 Kuchinoerabu-jima eruption. Here, we focus on the N-shaped TEC disturbances.

Strong disturbances can be seen only from GNSS stations located to the south of the volcano due to the interaction with geomagnetic fields (Heki, 2006). Therefore, we could not fully take advantage of the dense GNSS network because the Sakurajima, Shin-Moe and Kuchinoerabu-jima volcanoes are all located in southern Kyushu and GNSS stations are sparse to their south.

Following Heki (2006), we try to adjust a simple function

$$f(t) = -at\exp\left(\frac{-t^2}{2\sigma^2}\right), \qquad (1)$$

made of a set of positive and negative pulses, to the disturbances observed by five eruptions (Figure 4). This function has a maximum and minimum at t = -σ and t = σ, respectively (drawn as a smooth curve in red in Figure 4). The two parameters a and σ representing the amplitude and period, respectively, were tuned to minimize the root-mean-squares (rms) of differences between the synthesized and the observed disturbances.

We also move this function in time to find the optimal arrival time of the disturbance with the time step of 2.5 seconds. This procedure minimizes the influence from the temporally sparse data (30 second sampling). The values σ=19.5 resulted in good fits to the majority of time series, which corresponds to 78 seconds (1.3 minutes) as the approximate period (i.e. 4 × σ) of the disturbance. From the adjusted values of a, we obtained the peak-to-peak amplitude, i.e. $f(-\sigma)-f(\sigma)$, as summarized in Figure 5. Here we do not discuss the propagation velocity of the ionospheric disturbances because they are known to propagate in the acoustic wave velocity (~0.8 km/s) in the ionospheric F region (Heki, 2006). The same calculation

has been done for all the three examples from each eruption and the average peak-to-peak amplitudes are compared in Figure 5.

Volcanic eruptions excite acoustic waves in neutral atmosphere layer and ionospheric electrons move together with such neutral atmospheric molecules. Naturally, the strength of the TEC disturbances is largely influenced by the electron density in the F region of the ionosphere. As the index for the explosion intensity, it will be reasonable to normalize the amplitudes of STEC changes with background electron densities in the F region. Here we used background VTEC to normalize such amplitudes and express the TEC amplitudes relative to them (blue squares in Figure 5). VTEC values at the time and location of eruptions are obtained from GIM.

5. Discussion

To compare intensities of volcanic explosions, we often use VEI. They are either 3 (2015 Kuchinoerabu) or 2 (other 4 eruptions) for those studied here. VEI does not have finer scales and is not useful to compare intensities of explosive volcanic eruptions of this class. Intensities of volcanic explosions can be studied also by measuring amplitudes of airwaves (atmospheric pressure changes). However, different distance of the ground sensors from the volcanoes and different topographic and vegetation conditions makes it difficult to compare such intensities for different volcanoes.

In Fig. 5, we compare atmospheric pressure changes by the airwaves for the January 31 and February 11 explosions of the Shin-Moe volcano detected using the same sensor at the YNN station (JMA, 2011). These two eruptions show similar amplitudes of STEC changes. However, the background VTEC at the time of the February eruption was more than twice as strong as those in the January eruption. Hence, relative amplitude of the January eruption becomes twice as large as the February eruption. This is in agreement with the difference of the pressure changes for these two eruptions (458.5 Pa for the January 31 eruption, and 244.3 Pa for the February 11 eruption).

This suggests the validity of using the relative amplitudes of the ionospheric STEC changes as the new index to describe the intensities of volcanic explosions for different volcanoes. Its benefit is that we do not rely on the deployment of infrasound sensors, i.e. we can use this index whenever permanent GNSS networks are available on the southern/northern side of the volcano in northern/southern hemisphere.

Its drawback is that this index can be used only for strong volcanic explosions occurring when number of ionospheric electrons are sufficient (e.g., during daytimes). In fact, there were two explosions of the Shin-Moe volcano (Feb.1 20:25 UT, and Feb. 13 20:07 UT) with stronger airwaves than the February 11 02:36 UT eruption. However, we cannot find ionospheric disturbances for these explosions because of small background VTEC early in the morning (Figure S4).

We also looked for such TEC signatures outside Japan. However, we failed to add more cases due to the lack of GNSS stations in appropriate places or to the insufficient intensities of the explosions. The only

exception is the TEC signatures made by the human-induced explosion in 2020 August in Lebanon (Kundu et al., 2021).

At last, we discuss the origin of the period of the observed TEC variations. As seen in Fig. 3, TEC changes by the five different volcanic explosions have similar periods of ~ 1.3 minutes. Such a uniformity suggests its origin in the atmospheric structure rather than characteristics of the volcanic eruptions. In Fig. 6, we compare this period with the diagram of atmospheric attenuation of acoustic waves with various periods at different altitudes (Blanc, 1983).

Figure 6 shows that 1.3 minutes corresponds to the shortest period of the airwaves that can reach the altitude of ionospheric F region (~ 300 km) without large attenuations, i.e. 12.8 mHz corresponds to the high end frequency of the atmospheric band-pass filter. Infrasound records observed at ground sensors associated with explosive volcanic eruptions have stronger powers in periods much shorter than 1.3 minutes (e.g. Matoza et al., 2019). However, only those with periods 1.3–4.0 minutes can reach the ionospheric F region. Because the original spectrum had larger powers for higher frequencies, we would have detected the 12.8 mHz component as the TEC changes at the F region altitude.

Abbreviations

GEONET: GNSS Earth Observation Network

GIM: Global Ionospheric Map

GNSS: global satellite navigation system

GPS: Global Positioning System

IPP: ionospheric piercing point

LoS: line-of-sight

SIP: sub-ionospheric points

STEC: slant TEC

TEC: total electron content

VEI: Volcanic explosivity index

VTEC: vertical TEC

Declarations

Availability of data and materials

Due to confidentiality agreements, supporting data can only be made available to bona fide researchers subject to a non-disclosure agreement. Details of the data and how to request access please contact corresponding author

Competing interests

The authors declare that they have no known competing financial interests or personal relationships that could have appeared to influence the work reported in this paper.

Funding

This research was financed by the World Class Professor 2019 program by the Indonesian government and supported by JSPS KAKENHI Grant Number JP20K04120.

Authors' contributions

Mokhamad Nur Cahyadi: Conceptualization, Methodology, Formal analysis, Writing - review & editing, Investigation, Supervision.

Ririn Wuri Rahayu: Writing - original draft, Methodology, Formal analysis.

Eko Yuli Handoko: Formal analysis, Investigation

Kosuke Heki: Conceptualization, Methodology, Formal analysis, Writing - review & editing, Supervision.

Acknowledgements

We thank to reviewers for constructive reviews. This research was supported by the World Class Professor 2019 program by the Indonesian government, and by JSPS KAKENHI Grant Number JP20K04120.

Authors' information

Mokhamad Nur Cahyadi received the M.Sc. degree in Geomatics Engineering from Stuttgart University Germany in 2010, and the Ph.D degree in Natural History Sciences Laboratory from Hokkaido University, Japan in 2014. He is currently lecturer and researcher at Geomatics Engineering, Sepuluh Nopember Institute of Technology, Indonesia. His research interest includes developing Low-cost GPS, Navigation, and Ionospheric disturbance (TEC). He is currently supervising four master students and working on the project of ionospheric anomaly detection after earthquake.

Eko Yuli Handoko received the S.T. and M.T. degree in Geodesy engineering from the Bandung Institute of Technology, Indonesia, in 1998 and 2003 respectively, and the Dr. degree in surveying engineering from Universidade do Porto, Portugal in 2011. He is currently a Lecturer with the Department of Geomatics Engineering at Sepuluh Nopember Institute of Technology, Indonesia. His research focuses on Geodesy, GNSS meteorology, Sea Level Rise, Satellite Altimetry.

Ririn Wuri Rahayu received the S.T degree in Geomatics engineering from Sepuluh Nopember Institute of Technology, Indonesia in 2018. Her undegraduated thesis is focused on the effect of ionospheric correction on the results of single frequency gps coordinates using the klobuchar model. She is curently a master student at the same department and institute as S.T degree. Her recently research interest includes TEC anomaly detection after volcano and eartquake event.

Kosuke Heki is currently a Professor of Department of Earth and Planetary Sciences, Earth and Planetary Dynamics, Hokkaido University, Japan. He is a researchers of space geodesy, which highly interested in GNSS (e.g. GPS). He use GNSS to measure short-term crustal movements such as coseismic jumps as well as long-term motions reflecting plate tectonics and slow earthquakes. Measurement of ionospheric total electron contents with GNSS offered hot topics, e.g. constraint of the orbits and powers of ballistic missiles, discovery of changes in ionosphere immediately before large earthquakes.

References

1. Astafyeva, E. and K. Heki (2009) Dependence of waveform of near-field coseismic ionospheric disturbances on focal mechanisms, Earth Planet. Space, 61, 939-943
2. Blanc, E. (1985). Observations in the upper atmosphere of infrasonic waves from natural or artificial sources-A summary. In *Annales Geophysicae* (Vol. 3, pp. 673-687).
3. Cahyadi, M. N., Rahayu, R. W., Heki, K., & Nakashima, Y. (2020). Harmonic ionospheric oscillation by the 2010 eruption of the Merapi volcano, Indonesia, and the relevance of its amplitude to the mass eruption rate. *Journal of Volcanology and Geothermal Research*, *405*, 107047.
4. Chonan, M. et al., (2018). Ionospheric disturbances associated with Mt. Asama eruption observed by GPS-TEC and HF Doppler sounding, paper presented at the Japan Geoscience Union, General Assembly, Chiba, May 20-24, 2018.
5. Dautermann, T., Calais, E., Mattioli, G. S., (2009a). Global Positioning System detection and energy estimation of the ionospheric wave caused by the 13 July 2003 explosion of the Soufrière Hills Volcano, Montserrat. J. Geophys. Res., 114, B02202, doi:10.1029/2008JB005722.
6. Dautermann, T., Calais, E., Lognonné P., Mattioli, G. S., (2009b). Lithosphere-atmosphere-ionosphere coupling after the 2003 explosive eruption of the Soufriere Hills Volcano, Monserrat. Geophys. J. Int., 179, 1537–1546, doi:10.1111/j.1365-246X.2009.04390.x.
7. Global Volcanism Program, (2013). Volcanoes of the World, v.4.9.3, Venzke, E (ed.), Smithsonian Institution, Downloaded 01 Mar 2021. doi:10.5479/si.GVP.-VOTW4-2013.
8. Heki, K. (2006), Explosion energy of the 2004 eruption of the Asama Volcano, central Japan, inferred from ionospheric disturbances, Geophys. Res. Lett., 33, L14303, doi:10.1029/2006GL026249.
9. Heki, K., (2021). Chapter 5-3: Ionospheric Disturbances Related to Earthquakes in Advances in Ionospheric Research: Current Understanding and Challenges, Space Physics and Aeronomy, Volume 3, edited by C. Huang and G. Lu, pp.320, Wiley/American Geophysical Union, ISBN:978-1-119-50755-0.

10. Heki, K. and Ping, J.-S., (2005). Directivity and apparent velocity of the coseismic ionospheric disturbances observed with a dense GPS array, Earth Planet. Sci. Lett., 236, 845-855.
11. Hofmann-Wellenhof, B., Lichtenegger, H., and Wasle, E., (2008). GNSS-Global Navigation Satellite Systems, Springer, doi:10.1007/978-3-211-73017-1.
12. Japan Meteorological Agency (Kagoshima Local Meteorological Observatory, and Fukuoka District Meteorological Observatory), (2010). Volcanic activity of Sakurajima volcano – October 2009 – January 2010 -, Report to Coodinating Committee for Prediction of Volcanic Eruption, Japan, Report No.105. (in Japanese)
13. Japan Meteorological Agency (Fukuoka District Meteorological Observatory and Kagoshima Local Meteorological Observatory), (2013). The 2011 Eruptive Activities of Shinmoedake Volcano, Kirishimayama, Kyushu, Japan, Quarterly J. Seism., 77, 65-96. (in Japanese with English abstract)
14. Japan Meteorological Agency (Fukuoka District Meteorological Observatory and Kagoshima Local Meteorological Observatory), (2015). Volcanic activity of the Kuchinoerabu-jima in 2015, https://www.data.jma.go.jp/svd/vois/data/-tokyo/STOCK/monthly_v act_doc/fukuoka/2015y/509_15y.pdf. (in Japanese)
15. Komjathy, A., Galvan, D.A., Stephens, P. et al. (2012) Detecting ionospheric TEC perturbations caused by natural hazards using a global network of GPS receivers: The Tohoku case study. Earth Planet Sp 64, 24. https://doi.org/10.5047/eps.2012.08.003
16. Kundu, B., Senapati, B. Matsushita, A. and Heki, K., (2021). Atmospheric wave energy of the 2020 August 4 explosion in Beirut, Lebanon, from ionospheric disturbances, Sci. Rep.,11, 2793, doi:10.1038/s41598-021-82355-5.
17. Mannucci, A. J., Wilson, B. D., Yuan, D. N., Ho, C. H., Lindqwister, U. J., and Runge, T. F., (1998). A global mapping technique for GPS-derived ionospheric total electron content measurements, Radio Sci., 33, 565–582, doi:10.1029/97RS02707.
18. Matoza, R., Fee, D., Green, D., Mialle, P., (2019). Volcano infrasound and the international monitoring system in Infrasound Monitoring for Atmospheric Studies, edited by Le Pichon, A., Blanc, E., and Hauchecorne, A., pp.1023-1077, Springer, Cham, ISBN:978-3-319-75138-2.
19. Nakada, S., Yoshimoto, M., Koyama, E., Tsuji, H. and Urabe, T., (2005). Comparative study of the 2004 eruption with old eruptions at Asama Volcano and the activity evaluation, Kazan, 50, 303-313. (in Japanese with English abstract)
20. Nakashima, Y., (2018). Multi-sensor study of dynamics of atmospheric waves induced by volcanic eruptions. PhD Thesis, Hokkaido University.
21. Nakashima, Y., Heki, K., Takeo, A., Cahyadi, M. N., Aditiya, A. and Yoshizawa, K., (2016). Atmospheric resonant oscillations by the 2014 eruption of the Kelud volcano, Indonesia, observed with the ionospheric total electron contents and seismic signals, Earth Planet. Sci. Lett., 434, 112–116, doi:10.1016/j.epsl.2015.11.029.
22. Newhall, C. G. and Self, S., (1982). The volcanic explosivity index (VEI) – an estimate of explosive magnitude for historical volcanism, J. Geophys. Res., 87, 1231-1238.

23. Occhipinti, G., Rolland, L., Lognonné, P., Watada, S., (2013). From Sumatra 2004 to Tohoku-oki 2011: The systematic GPS detection of the ionospheric signature induced by tsunamigenic earthquakes. J. Geophys. Res. Space Phys., 118, 3626O, doi:10.1002/jgra.50322.
24. Rolland, L. M., Vergnolle, M., Nocquet, J.-M., Sladen, A., Dessa, J.-X., Tavakoli, F., Nankali, H. R., and Cappa, F., (2013). Discriminating the tectonic and non-tectonic contributions in the ionospheric signature of the 2011, Mw7.1, dip–slip Van earthquake, Eastern Turkey, Geophys. Res. Lett., 40, doi:10.1002/grl.50544.
25. Shults, K., Astafyeva, E., Adourian, S., (2016). Ionospheric detection and localization of volcano eruptions on the example of the April 2015 Calbuco events. J. Geophys. Res. Space Physics, 121, 10,303–10,315, doi:10.1002/2016JA023382.
26. Yokoo, A., Maeno, F., and Taniguchi, H., (2005). Asama explosion of September 1st, 2004 – On the damage to glass windows and estimation of explosion energy, Kazan, 50, 195-201. (in Japanese with English abstract)

Figures

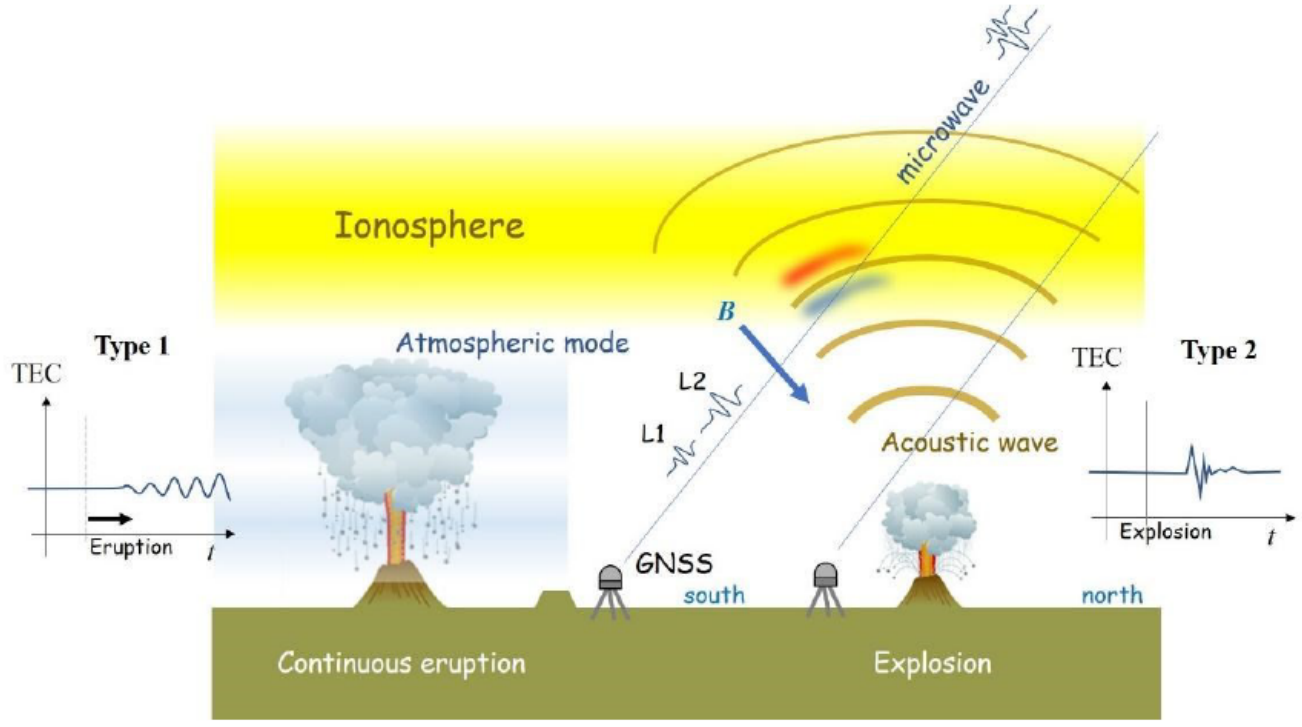

Figure 1

Ionospheric disturbance caused by continuous (Type 1 left) and explosive (Type 2 right) volcanic eruptions can be detected by differential ionospheric delays of microwave signals of two carrier frequencies (L1 and L2) from GNSS satellites. Strong continuous eruptions sometimes excite

atmospheric modes and long-term oscillatory disturbances in ionosphere. For explosive eruptions, we often find short-term impulsive disturbances in ionosphere 8-10 minutes after eruptions, the time required for acoustic waves to reach the ionospheric F region. The acoustic wave makes electron density anomalies (pairs of positive and negative anomalies as shown with red and blue colors in the figure) on the southern side of the volcano (for northern hemisphere cases).

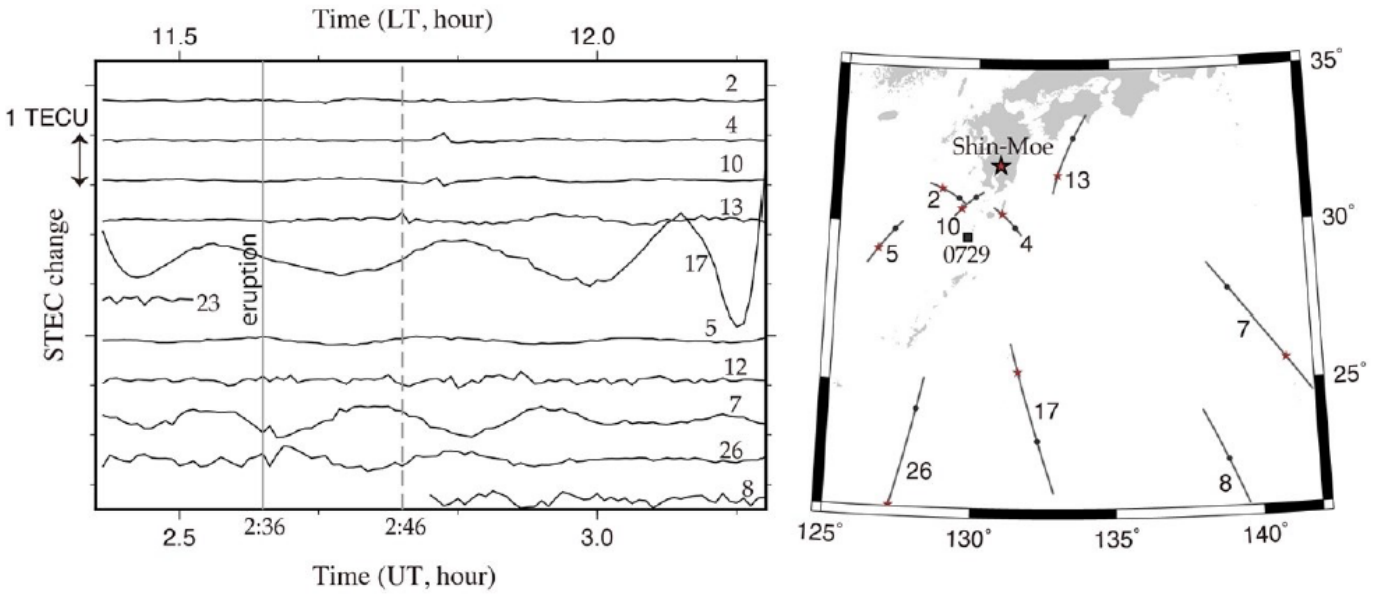

Figure 2

STEC changes observed at the GNSS station 0729 (square in the map) over 2.4-3.2 UT, February 11, 2011. An explosive eruption of the Shin-Moe volcano (star in the map) occurred at 2:36 UT (solid vertical line), and small ionospheric observations are seen to occur in signals with GPS satellites 4, 10, and 13 around 10 minutes after the eruption (dashed vertical line). In the map, we show the trajectory of SIPs with solid circles and red stars indicating the 3:00 UT and 2:36 UT, respectively. The same data on the previous and the next days are shown in Figure S3.

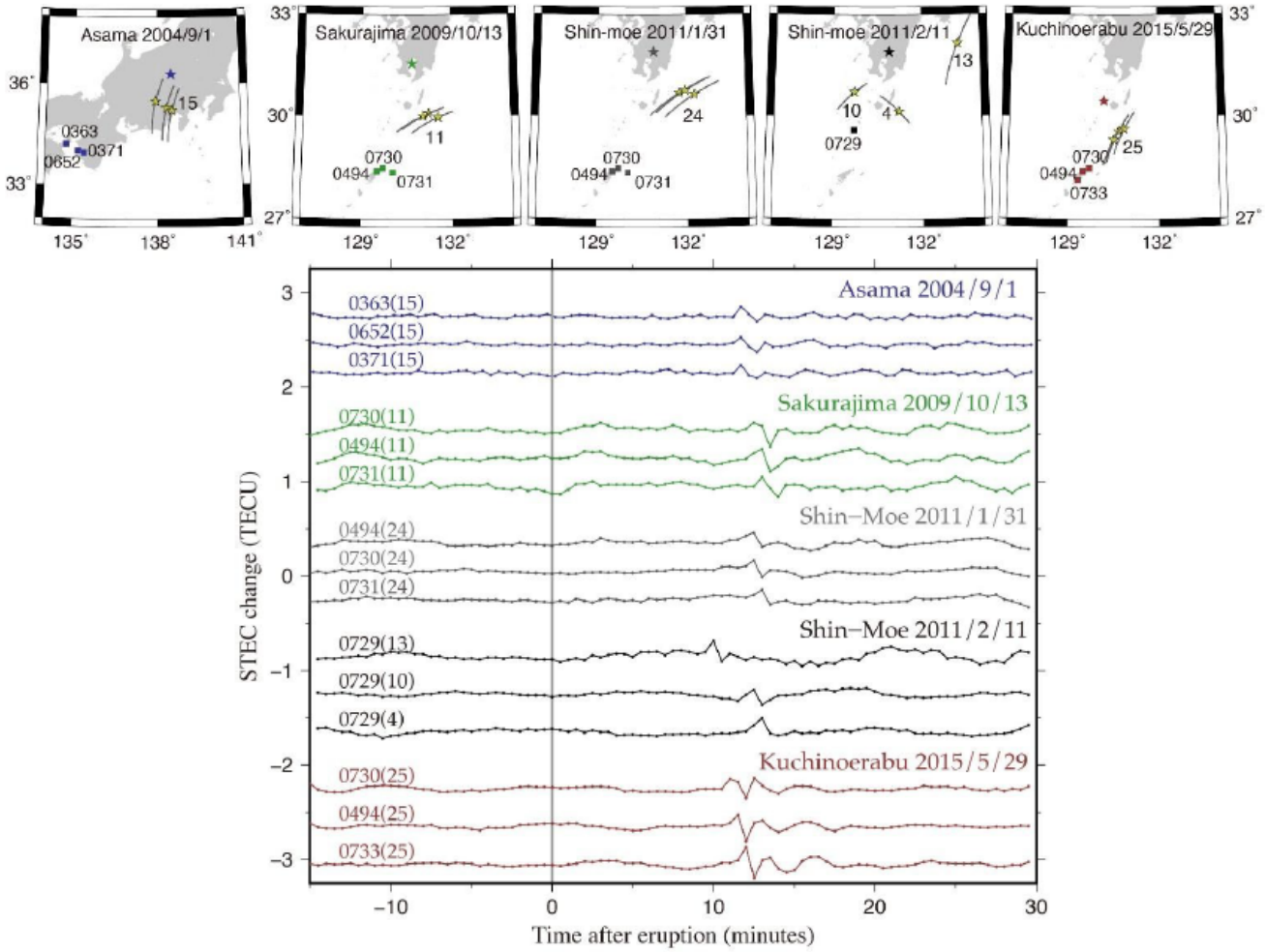

Figure 3

(top) Geometry of volcanoes (large stars), SIP tracks (gray curves) and SIP positions at the time of the eruptions (small yellow stars), and GNSS stations (squares). We show the STEC time series for the three pairs of stations and satellites (three satellites from one station for the second Shin-Moe eruption, and one satellite from three stations for the rest) for each of the five examples of explosive eruptions in Japan. (bottom) STEC changes after removing the long-period changes over 45 minutes periods (from 15 minutes before eruption to 30 minutes after eruption) for the five cases studied here. Small disturbances can be seen ~10 minutes after the eruptions.

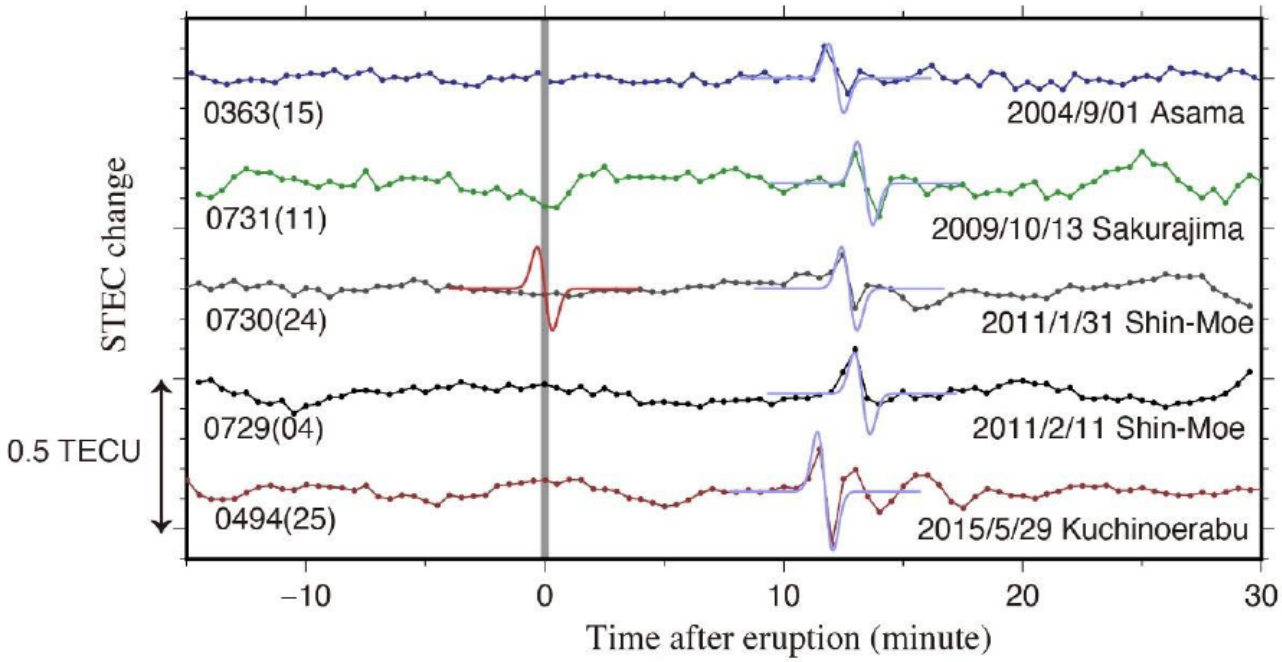

Figure 4

Fit of the model function (shown as a red curve in the middle) to one of the STEC curves in Figure 3 for each eruption. The period of the TEC fluctuation (Heki, 2006) is fixed to 1.3 minutes, and adjusted the amplitudes and time lags to minimize the difference between the model function and the observed TEC.

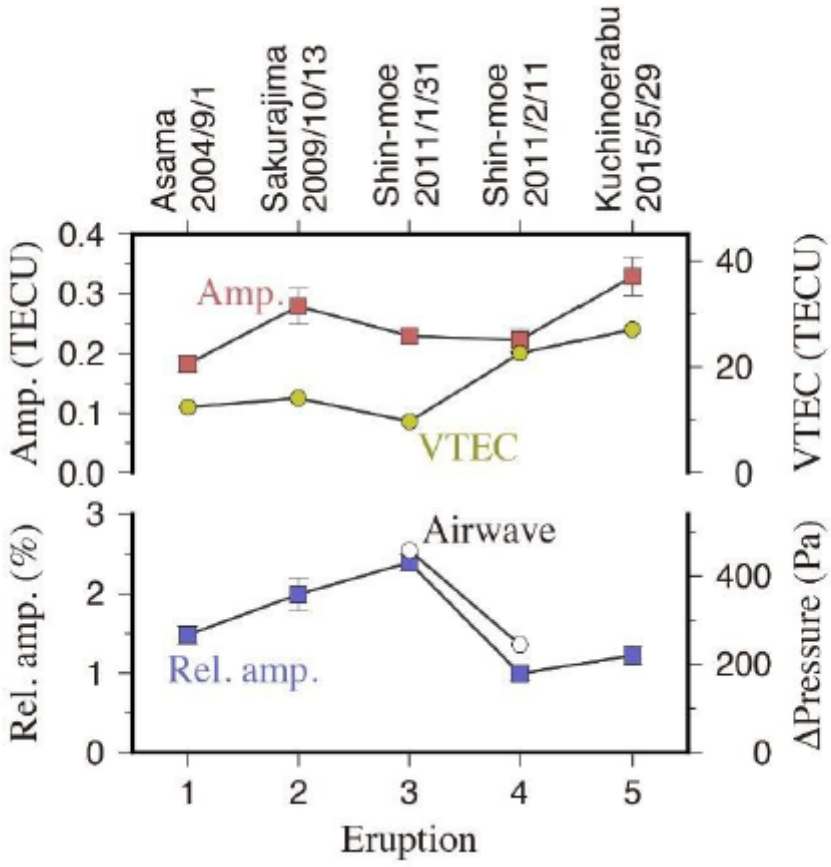

Figure 5

Comparison of the TECs (shown in Figure 3) in absolute (red) and relative (to the background VTEC) (blue) amplitudes. The yellow circles show VTEC values at the time and place of the eruptions calculated using GIM. For the two eruptions of the Shin-Moe volcano, we compare amplitudes of atmospheric pressure changes detected by the same sensor ~2.6 km from the volcano caused by airwaves of the explosions.

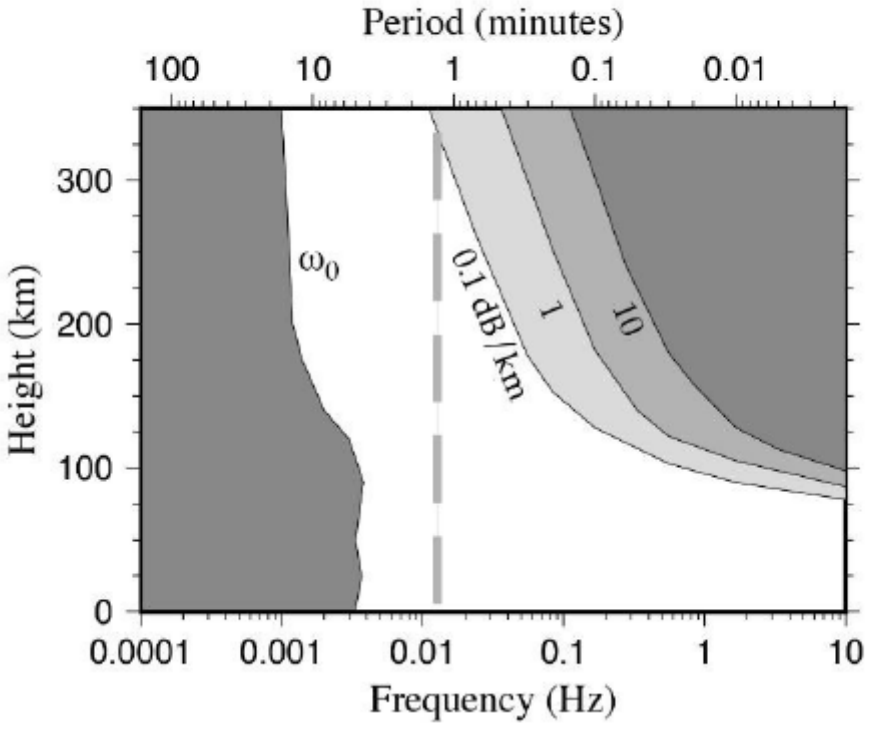

Figure 6

Frequency (~12.8 mHz) and period (~1.3 minutes) of TEC oscillations by explosive volcanic eruptions (vertical dashed line) drawn over the figure by Blanc (1983) showing the attenuation of airwaves in the Earth's atmosphere. The frequency 12.8 mHz corresponds to the higher end of the atmospheric bandpass filter.

Supplementary Files

This is a list of supplementary files associated with this preprint. Click to download.

- FigureS1.pdf
- FigureS2.pdf
- FigureS3.pdf

- FigureS4.pdf
- abstractfigureedit.jpg